Kemal Yaman ✉
Zafer Tekiner

https://doi.org/10.21278/TOF.503085425
ISSN 1333-1124
eISSN 1849-1391

A HYBRID FEM-GA-ANN MODEL FOR SPRINGBACK PREDICTION IN AIR V-BENDING OF AISI 1030 STEEL

Summary

This study examines springback in mild-steel sheet air V-bending through an integrated experimental-numerical-data-driven framework aimed at practical bend design and tool compensation. Bending tests were performed using a modular die set while systematically varying sheet thickness, punch radius, and target bending angle, and repeated measurements were used to ensure reliable springback evaluation. The experimental trends were cross-checked with nonlinear finite element simulations in MSC Marc Mentat®, providing a physics-based reference and confirming that the selected parameters govern the springback response over the investigated range. To enable fast prediction without repeated simulations, a feedforward artificial neural network (ANN) was trained on 106 experimental cases to map the forming parameters to springback. Because conventional ANN training can be sensitive to random initialisation and can become trapped in local minima, a genetic algorithm (GA) was employed to optimise the initial weights and biases prior to gradient-based learning. Compared with a standard ANN, the GA-optimised ANN delivered more stable convergence and improved generalisation, increasing test accuracy (R^2 from 0.833 to 0.875) and reducing the mean absolute error from 0.195° to 0.075° (61.5% improvement). Overall, the proposed hybrid approach combines experimental reliability, FEM validation, and GA-enhanced learning to provide an efficient and robust springback prediction tool for sheet-metal forming applications.

Key words: *air V-bending; springback; artificial neural network; genetic algorithm; cold forming; finite element analysis*

1. Introduction

A review of industrial manufacturing practices indicates that cold sheet metal forming remains one of the dominant production routes for mechanical components. Mild steel sheets are widely used in household appliances, automotive manufacturing, and electronic goods due to their favourable mechanical behaviour and good formability [1–2]. In these applications, tight dimensional tolerances require high geometric accuracy during forming. In practice, bending dies often undergo repeated adjustments to obtain the target geometry, which can increase cycle time, labour demand, and production cost [2]. Common bending operations include V-bending, U-bending, edge bending, and air bending. Inamdar et al. [3] investigated springback in air V-bending for five sheet materials. Their statistical analysis showed that the die-opening-to-thickness ratio and the bending angle have a strong influence on springback.

Although fewer in number, analytical studies have also clarified key mechanisms. The reported results indicate that bending curvature and die-punch geometry significantly influence elastic recovery after unloading [4]. Leu and Zhuang [5] proposed an empirical model for high-strength steel sheets incorporating thickness ratio, a strain hardening exponent, and anisotropy via Hill's anisotropic plasticity theory, and obtained reasonable agreement with experiments. Additional work has examined punch radius and sheet thickness effects in free V-bending. Hai et al. [6] bent SS400 specimens at 90°, 123.5°, and 150° with a 42 mm punch radius and observed increased springback with increasing bend angle. Asnafi [7] studied thick stainless-steel sheets (7.9–31.3 mm) and developed an analytical model predicting a springback angle together with an inner radius and minimum die width before unloading; despite some deviations, overall agreement was satisfactory.

Streppel et al. [8] reported that analytical models can lose validity under industrial conditions, especially with small punch radii and large die openings. Such models may still support process planning, yet they often neglect influential factors including die geometry details, yield behaviour, and the Bauschinger effect [9]. These inherent limitations of closed-form analytical approaches motivated the adoption of numerically based methods capable of resolving complex contact conditions and nonlinear material responses. With improved computational resources, the Finite Element Method (FEM) has therefore been widely adopted for springback analysis [10–14]. FEM provides detailed predictions but typically requires advanced constitutive input and notable computational time, limiting its usefulness for rapid design iterations. Tekiner [10] performed extensive experiments using modular air V-bending dies across different materials and geometries (about 1000 tests per configuration) and quantified the effects of dwell time, punch depth, and die geometry; longer contact times reduced springback.

Other studies have highlighted rolling direction, heat treatment, and tool geometry effects. Badr et al. [14] reported substantially lower springback in rolled Ti-6Al-4V sheets than in unrolled ones. V-bending tests on 1.2 mm SCGADUB1180 steel showed minimum springback at small punch radii and high bending angles, and maximum values at low bending angles with larger punch radii; alignment with the rolling direction improved bendability and reduced springback [15]. Rolling speed and heat treatment also significantly influence springback [16–18]. Although FEM addresses the deficiencies of analytical models, its computational cost and sensitivity to constitutive assumptions restrict its direct use in iterative process design. These constraints have therefore driven interest in faster, data-driven surrogate methods. As data-driven strategies have expanded, artificial intelligence methods have been explored as alternatives.

Artificial Neural Networks (ANNs) are attractive for springback prediction because they can learn nonlinear relations among material behaviour, tool geometry, and process parameters. Conventional backpropagation-based ANNs have provided reliable estimates in air V-bending when trained with sufficiently representative datasets [19]. Training set composition is critical, and improved performance has been reported for networks trained on thinner sheets, particularly 2 mm data [20]. Experimental studies varying thickness, die opening, and holding time reported ANN models outperforming Multiple Linear Regression under interacting conditions [21]. However, classical architectures can suffer from overfitting and local convergence issues [22–23]. Hybrid ANN approaches using evolutionary optimisation have been introduced, and GA-assisted ANN models have improved convergence and robustness for anisotropic steels and plate bending applications [24–25]. More recent research has integrated FEM-generated datasets and advanced machine-learning frameworks to capture complex geometric-mechanical interactions [26]. Experimental evidence also supports the combined effects of multiple forming parameters in nonlinear modelling approaches [27-28].

Taken together, these findings indicate a clear progression in springback modelling, where analytical approaches provide physical insight, FEM ensures geometric and constitutive fidelity, and ANN-based methods improve computational efficiency, although each method presents limitations when applied independently, encouraging the development of integrated frameworks. The present study proposes an integrated framework combining experiments, FEM, and a GA-optimised ANN (GA-ANN) to predict springback in air V-bending of mild steel sheets. Since FEM accuracy depends on constitutive assumptions and given that conventional ANN training is prone to local convergence issues [29–31], GA-based optimisation is employed to enhance learning stability and reduce prediction variability [32–33]. Unlike approaches that treat these tools separately, this study exploits their complementarity within a unified scheme, improving generalisation against nonlinear coupling among thickness, tool geometry, and loading conditions [34], and offering a practical route for reducing springback-related deviations in industrial forming.

The key contribution of this study is the integration of experimentally validated FEM data with a GA-optimised ANN, where GA improves not only training speed but also model stability by reducing the sensitivity to random weight initialisation, a limitation commonly overlooked in conventional ANN-based springback studies.

2. Air V-bending

In air bending, the sheet metal part is supported by the edges of the mould located below. This support method plays a critical role in ensuring that the sheet metal part reaches the desired form. The downward movement of the punch according to the die distance creates the bending effect on the sheet material. This bending effect results in the punch creating the necessary bending angle by applying pressure. As seen in Fig. 1, R_p is the punch radius, R_d is the die radius, θ is the bending angle, and θ' is the angle measured after springback. Although the air bending process is similar to V-bending in terms of the shape the sheet metal part takes, it has some important differences. In particular, the edges of the sheet metal part are free at the beginning and end of the bending process. This freedom allows the sheet metal to move without experiencing any compression or deformation while coming to the desired form. The air bending process is particularly useful in obtaining complex shapes. The free edges of the sheet metal provide more flexibility and control during the bending process [1].

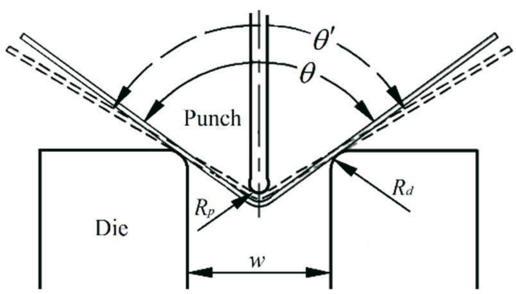

Fig. 1 Nomenclature of air V-bending [11, 23]

Correct alignment of the die and punch is critical to the success of the bending process. Misalignment can cause the sheet metal to deviate from the desired form or cause unexpected deformations. Therefore, careful adjustment of the die and punch is necessary during the bending process. These adjustments determine how the sheet metal will move during the bending process and its final form. [1, 11, 23].

In air bending dies, a linear bending profile is not observed at the initial stage of deformation. As illustrated in Fig. 2, the punch forms a curved, non-linear bending shape over the freely supported sheet due to material response. Linearity begins to appear only after the deformation progresses toward the die shoulders [1]. More specifically, free bending produces a non-linear curvature because the punch pressure is concentrated in the central region, while the sheet edges remain unsupported. This causes greater deformation beneath the punch and a gradual decrease toward the edges. The process starts with elastic deformation at the punch-sheet contact zone and transitions into plastic deformation; however, the deformation is not uniformly distributed along the punch width.

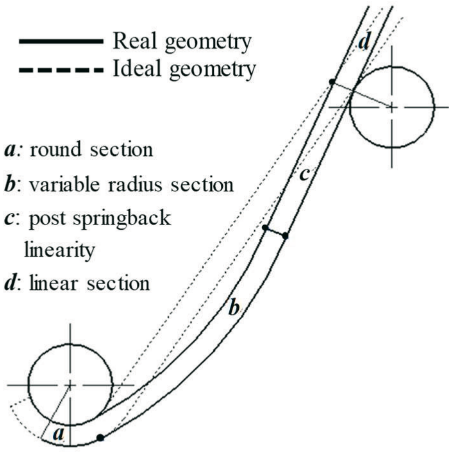

Fig. 2 Sheet sections formed in air V-bending [1]

As the material approaches the die edges, the applied force diminishes, leading to a more uniform stress state and a nearly linear bending profile in these regions. Material properties such as thickness, hardness, and elastic-plastic behaviour also influence this curvature formation. Consequently, while the centre exhibits a pronounced non-linear bending curve due to varying stress and deformation distribution, the bending shape becomes more stable and linear near the die edges [1].

3. Experimental work

In the bending experiments, rectangular specimens with dimensions of 60 × 20 mm were used. These dimensions were selected to ensure adequate bending moment development and reliable springback measurement while minimising edge effects and maintaining geometric stability. DKP (DC01, EN 10130 – AISI 1010) mild steel sheets with thicknesses of 1, 2, 3, and 4 mm were bent at bending angles of 15°, 30°, 45°, 60°, 75°, 90°, and 120°. Although three bending radii were employed for each thickness, these radii were not constant; instead, they were selected in proportion to sheet thickness to maintain comparable R/t ratios and ensure consistent deformation behaviour (e.g., for $t = 4$ mm, $R = 4$, 6, and 8 mm). All sheets were used in their as-received cold-rolled condition, and specimens were cut from the same batch and aligned parallel to the rolling direction to ensure material consistency. The tensile tests for the witness specimen, produced from the same batch and bearing the same serial number as the bending samples, were carried out using an H300KU Tinius Olsen tensile testing machine in accordance with the ASTM E8-M standard. These tests provided the essential mechanical properties of the material, including the modulus of elasticity, the yield strength, and the ultimate tensile strength. The geometric dimensions of the dog-bone specimen and the stress-strain curve obtained from the tensile test are shown in Fig. 3. Predicting the exact variation of springback is challenging due to the many interacting material and process parameters.

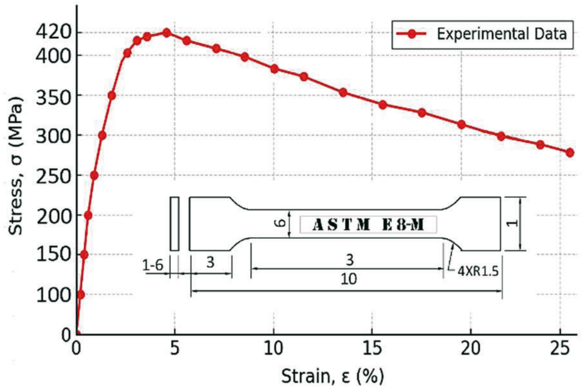

Fig. 3 Stress-strain curve of the DKP steel specimen and the ASTM E8-M tensile specimen geometry

Factors such as heat treatment and rolling direction influence the reproducibility of the tensile test results, even when the tests are conducted under identical conditions. For this reason, all specimens were prepared in the same drawing direction and taken from the same production batch to maintain consistency throughout the experiments.

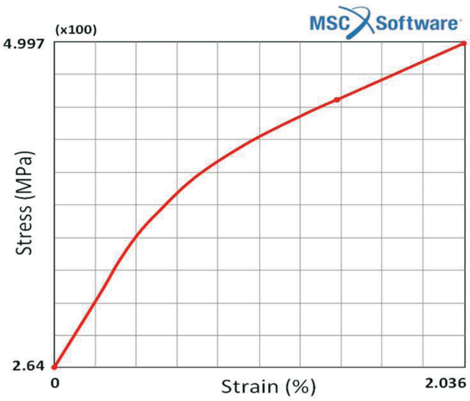

Fig. 4 True stress-plastic strain graph of DKP steel material

The bending process was carried out numerically with the MSC Marc Mentat® analysis programme. In order to define the material, three tensile tests were performed on the samples at standard values and the stress-strain graph for DKP steel shown in Fig. 4 was obtained according to the average values obtained. The values in Table 1 were used as analysis input data to define the material. In the numerical model, the material was represented using an isotropic elastic-plastic model with bilinear hardening. This approach is appropriate for DKP (DC01) mild steel, as its low anisotropy and limited Bauschinger effect allow uniaxial tensile data to capture the dominant plastic response. The elastic properties (E = 200 GPa, v = 0.3) were taken from the experimental data, and the plastic region was modelled using the true stress-strain curve derived from the same tensile test batch. This curve was defined in the MSC Marc Mentat software as a user-input material table to ensure accurate representation of the nonlinear deformation behaviour during bending and springback.

Table 1 Physical properties of DKP steel used in numerical analysis

Modulus of Elasticity (E)	Poisson ratio (v)	Density (ρ)	Yield stress (σ_y)	Ultimate tensile strength (σ_{UTS})	Tangent modulus (E_t)	Strain hardening exponent (n)
200 GPa	0.3	7.8 g/cm^3	256 MPa	424 MPa	5 GPa	0.18

To support the numerical analysis, the plastic behaviour of the DKP steel was modelled using a bilinear isotropic hardening law. The material model includes an initial elastic region followed by a linear hardening region. This relationship can be expressed as:

$$\sigma(\varepsilon)=\begin{cases} E\cdot\varepsilon, & for\,\varepsilon\leq\varepsilon_y \\ \sigma_y+E_t\left(\varepsilon-\varepsilon_y\right), & for\,\varepsilon>\varepsilon_y \end{cases}, \tag{1}$$

where E=200 GPa is the Young's modulus, σ_y=250 MPa is the yield strength, E_t=5 GPa is the tangent modulus determined from the slope of the true stress-strain curve beyond yielding, and ε_y (σ_y/E) is the yield strain. This equation was used in cases where the full stress-strain curve was approximated analytically. It complements the user-defined material curve provided in Fig. 4 and improves the interpretation of the numerical simulation results. In the finite element simulations, a Coulomb friction model was also used to describe the contact between the punch, die, and the sheet metal surfaces, with a constant coefficient of friction for dry contact conditions.

Table 2 Mesh convergence analysis values

Mesh level	Number of elements	Predicted $\Delta\theta$ (deg)	Difference (%)
Coarse	768	1.842	-
Medium	1024	1.791	2.77
Fine	1536	1.768	1.28

In the finite element model, the sheet was discretised using 1024 quadrilateral four-node shell elements with an average in-plane element size of 0.8 mm in the bending zone and 1.5 mm in far-field regions. Mesh refinement was concentrated at the punch contact area to accurately capture stress gradients governing springback. A convergence study comparing 768, 1024, and 1536 elements confirmed that further refinement beyond 1024 elements yields springback angle differences below 1.2%, validating the selected mesh density as both accurate and computationally efficient (Table 2). Contact between the punch, die, and sheet was modelled using a Coulomb friction formulation. A friction coefficient of μ = 0.125 was adopted, consistent with values reported in the literature [11, 12, 26] for dry steel-on-tool contact in sheet metal bending operations. Material behaviour was introduced through experimentally derived true stress-plastic strain data together with a bilinear isotropic hardening law. A large deformation implicit analysis was carried out in MSC Marc Mentat, and automatic contact stabilisation enhanced convergence during loading and unloading. Boundary conditions replicated the experimental setup, with the die fully constrained and the punch driven by a prescribed displacement. This modelling strategy provided a realistic representation of deformation and enabled close agreement between simulated and experimental springback values, and a mesh-independence check showed $\Delta\theta$ differences below 2%.

Mould dimensions were determined based on experimental approaches reported in the literature. The mould was manufactured using CNC milling, 4-axis wire EDM, and conventional machining equipment, with wire EDM ensuring high dimensional precision of the modular components. Bending tests were conducted on a double-acting hydraulic press. Springback angles were measured after each test using an optical projection device (±0.1° resolution, ±0.05° repeatability) and used in all subsequent analyses. No dwell time was applied; the punch was retracted immediately after reaching the target displacement.

4. Results and discussion

This section presents a comparative evaluation of the experimental and numerical results obtained from air V-bending tests performed on 1 mm thick sheet metal. Springback behaviour is analysed under varying bending angles and punch radii using both experimental measurements and finite element method (FEM) simulations. The results highlight the relationship between bending parameters and residual deformation and aim to validate the accuracy of the FEM model through consistent trends and deviations observed at critical angles. When the graphs are investigated, the numerical analysis and experimental springback values are presented comparatively in Figs. 5 and 8. Figure 5 demonstrates close agreement between the experimental and FEM bending results for the 1 mm sheet.

In general, the variation of springback increases with the increasing bending angle, while the experimental measurements exhibit a low dispersion, with a standard deviation of approximately 5%. For example, for a nominal bending angle of 15°, the experimentally measured final angle after unloading was 17.58°, whereas the finite element analysis (FEA) predicted a value of 18.07°. Accordingly, the springback variations ($\Delta\theta = \theta_{\text{final}} - \theta_{\text{nominal}}$) were 2.58° for the experimental case and 3.07° for the numerical model (Fig. 6).

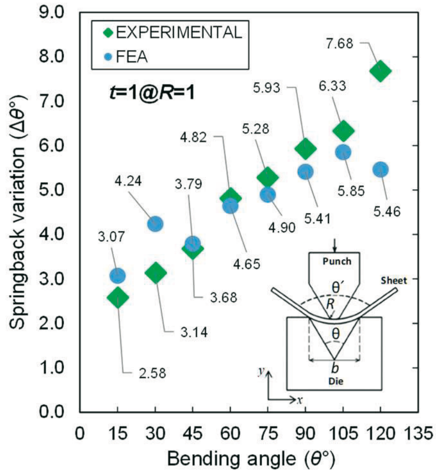

Fig. 5 Experimental-FEM comparison of air V-bending for 1 mm DKP sheet

At a bending angle of 120°, the experimentally measured final angle increased to 125.85°, while the FEA prediction was 127.68°. Thus, the corresponding springback magnitudes increased to 5.85° (experimental) and 7.68° (numerical).

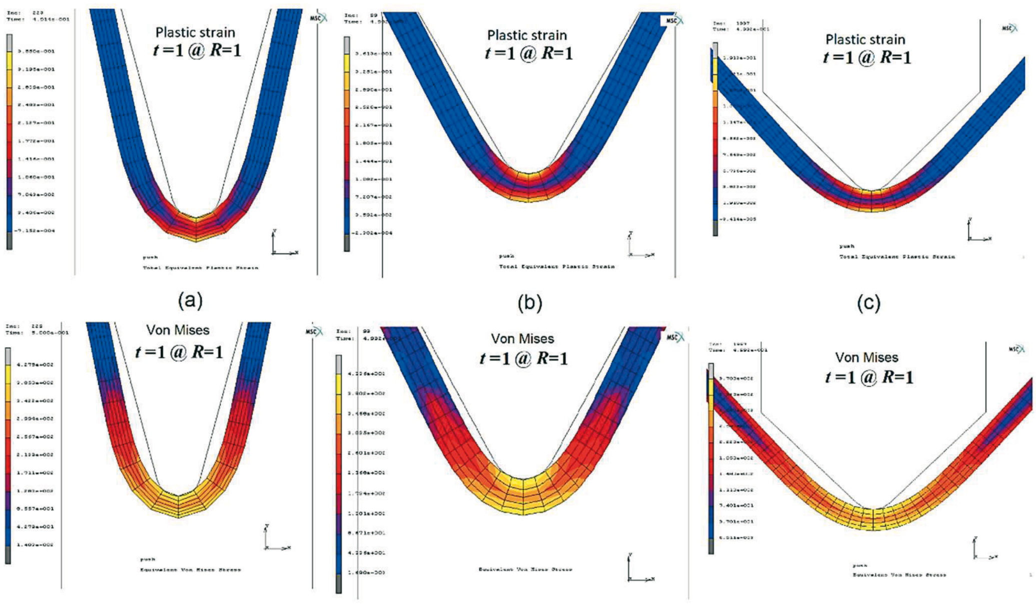

Fig. 6 FEM springback (stress) for a 1 mm sheet at (a) 30°, (b) 60°, and (c) 90° (R = 1–3 mm)

This comparison clearly shows that both the experiment and the numerical models exhibit a consistent trend in which springback increases with the increasing bending angle, a behaviour that becomes more pronounced as the punch penetration depth increases due to the higher strain accumulation in the sheet. It is evident that the springback (measured angle) increases with the bending angle, as illustrated in Fig. 5. For the sake of brevity, only the FEM results corresponding to bending angles of 30°, 60°, and 90° are presented in this section. Figures 6a–6c show that although the magnitude of plastic deformation decreases at larger bending angles due to shallower punch penetration, the springback variation increases as the elastic moment arm becomes longer.

When the Von Mises stress values under constant sheet thickness and punch radius are examined, it can be seen that increasing the nominal bending angle leads to a shallower punch penetration, causing the plastic strain to decrease and the stress distribution to spread over a wider region with reduced intensity. Although lower plastic deformation results in lower peak stress levels, the variation of springback increases because the effective bending arm becomes longer and elastic recovery becomes more dominant at larger bend angles. Figure 7 presents the equivalent Von Mises stress distribution for the 1 mm thick sheet bent with a 1 mm punch radius, illustrating these variations in detail.

When the bending results of the 1 mm thick sample with a punch radius of 2 mm were examined, springback increased as the bending angle increased compared to the bending results with a punch radius of 1 mm, while the experimental measurements exhibited a standard deviation of approximately 5%, indicating acceptable repeatability. However, an increase in springback values was observed as the punch radius increased (Fig. 8).

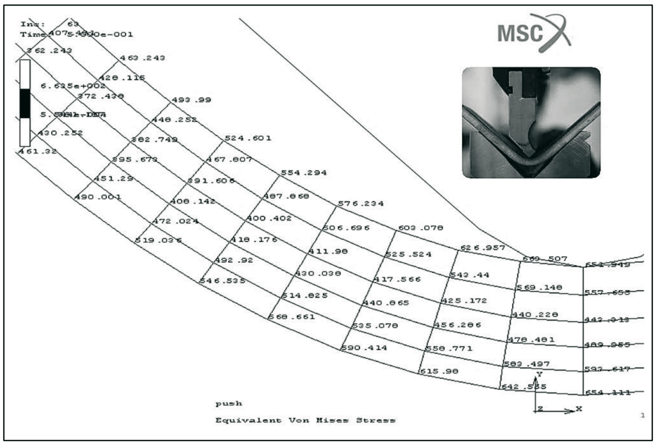

Fig. 7 Von Mises stress distribution of the semi-model at 90° bending (1-mm DKP, R_p = 1 mm)

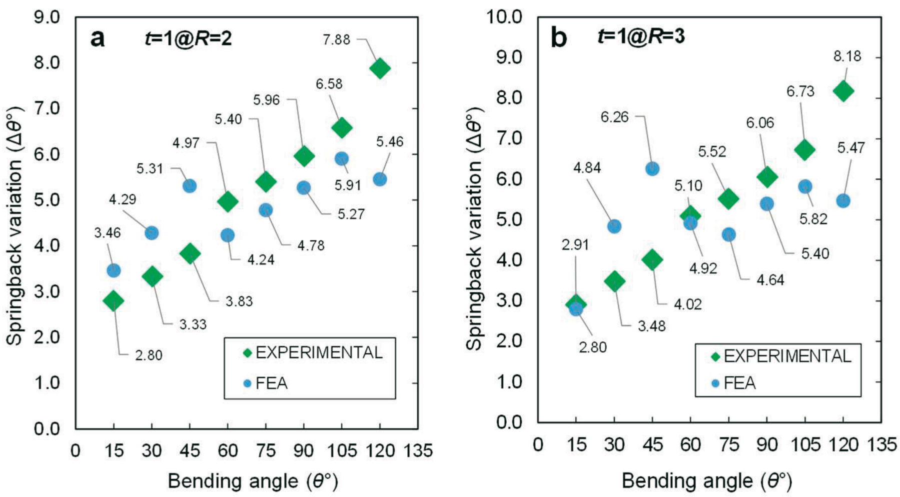

Fig. 8 Experimental-FEM comparison of air V-bending for t = 1 mm sheets with (a) R = 2 and (b) R = 3

Figures 8a and 8b show that the experimental and FEM springback results follow a similar overall trend; however, deviations become more pronounced at bending angles of 45° and 120°. At 45°, the elastic-plastic transition zone is highly sensitive, and local material anisotropy or minor experimental misalignments may contribute to the observed differences. At wider bending angles such as 120°, it is considered that since the material undergoes less plastic deformation, the springback becomes more dependent on elastic recovery, and it is presumed that this situation is more affected by assumptions such as friction, boundary conditions, and mesh density used in the FEM model. In addition, in the finite element analyses, an idealised isotropic hardening behaviour was adopted together with a constant Coulomb friction coefficient (μ = 0.125). Although this approach is sufficient to reflect the overall behaviour, it may not fully capture the local variations corresponding to extreme bending angles. Nevertheless, the FEM results show that springback increases with the bending angle and punch radius, thereby demonstrating the consistency of the numerical model with experimental observations. Figure 9 illustrates the finite element analysis (FEA) results of plastic strain distribution for 1 mm thick sheet metal during air V-bending at bending angles of (a) 30°, (b) 60°, and (c) 90°, using punch radii of 1 mm, 2 mm, and 3 mm. The colour scale, ranging from red to blue, represents the magnitude of equivalent plastic strain.

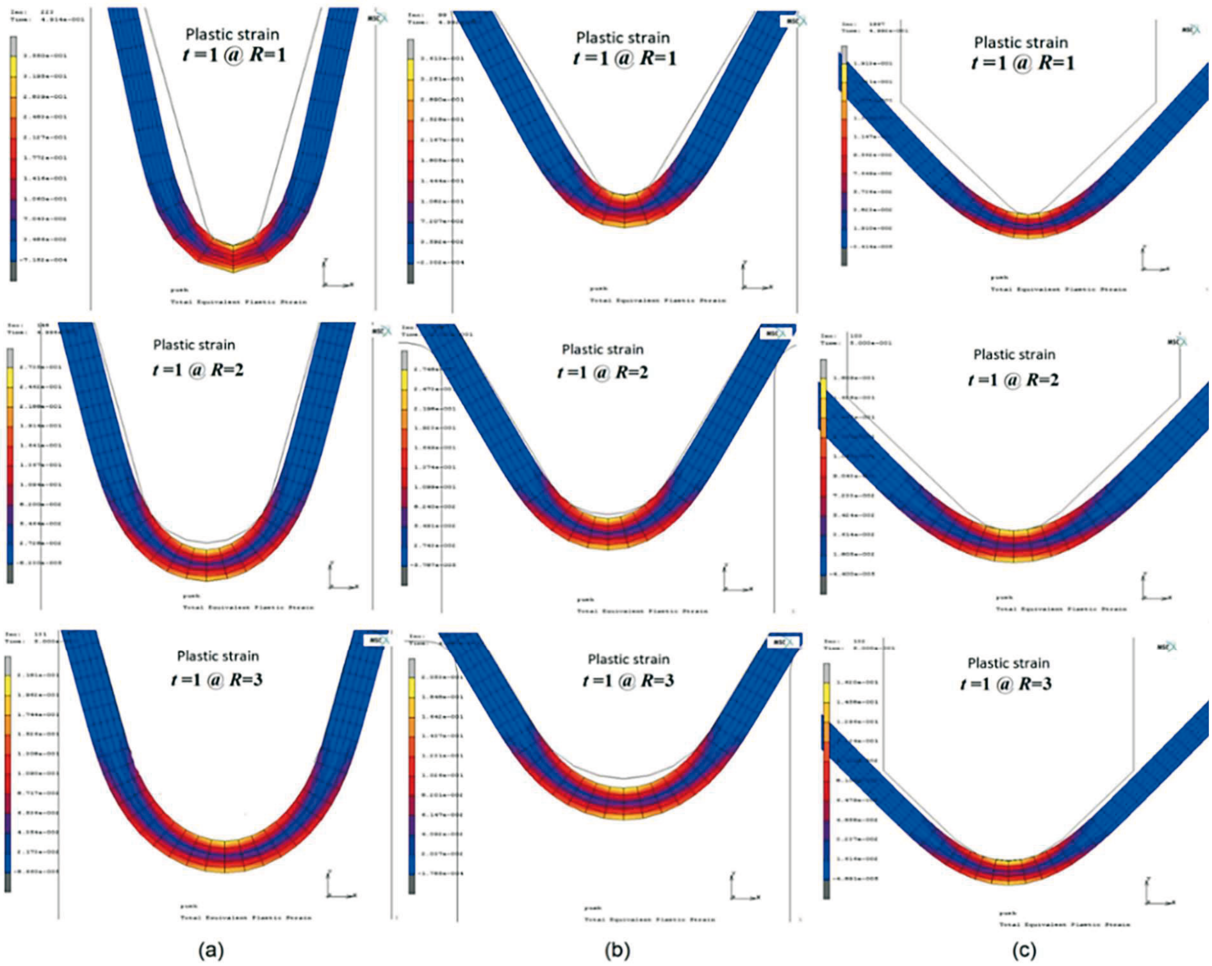

Fig. 9 FEM springback (strain) for a 1 mm sheet at (a) 30°, (b) 60°, and (c) 90° (R = 1–3 mm)

As the bending angle increases, the plastic strain spreads over a larger area, indicating greater material deformation at wider angles. Additionally, increasing the punch radius results in a more uniform strain distribution with a reduction in peak plastic strain values at the bend apex. This suggests that larger punch radii reduce stress concentration and promote a smoother deformation process.

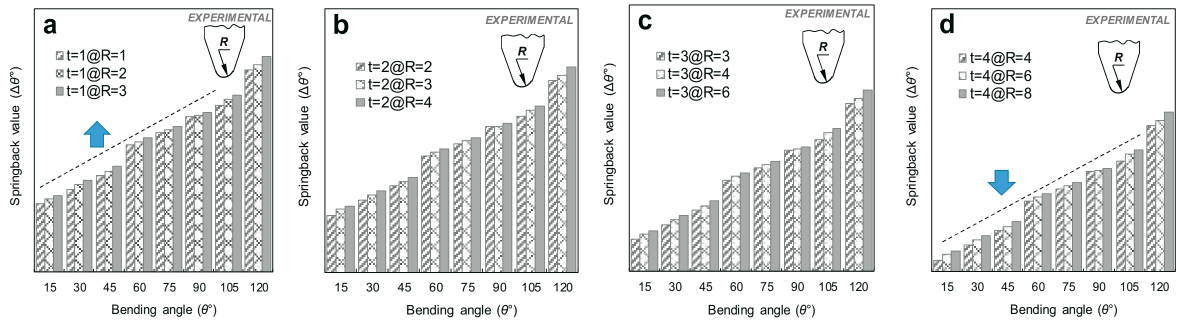

Fig. 10 Experimental comparison of the air V-bending process for (a) 1 mm, (b) 2 mm, (c) 3 mm and (d) 4 mm thick DKP sheet under variable punch radii

These results are crucial for understanding and predicting springback behaviour in sheet metal forming and can guide the selection of optimal tool geometry to minimise dimensional inaccuracies. Consistent with previous studies [3, 5–21], the present results show that increasing sheet thickness reduces springback because a larger proportion of the cross-section undergoes plastic deformation during bending. Figure 10 demonstrates an approximately linear increase in springback with an increasing bending radius for a given sheet thickness. While springback increases as the bending angle increases, the lengths of the column bars gradually shorten from Fig. 10a to Fig. 10d in the graphs. Therefore, as the sample thickness increases, the springback values also decrease.

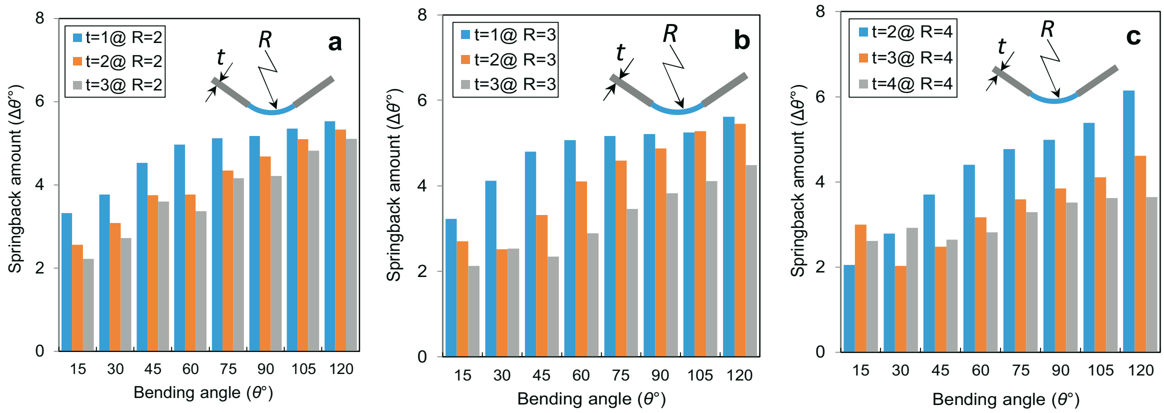

Fig. 11 Experimental comparison of the air V-bending process for constant (a) R=2 mm, (b) R=3 mm and (c) R=4 mm sample punch radius under variable (1, 2 and 3 mm) sheet thickness

Figure 11 presents the experimental comparison of springback variations ($\Delta\theta°$) during the air V-bending process for different sheet thicknesses (t = 1, 2, 3, and 4 mm) at constant punch radii: (a) R = 2 mm, (b) R = 3 mm, and (c) R = 4 mm. In general, the variation of springback increases with the bending angle, indicating that materials tend to exhibit more elastic recovery at greater angles. Additionally, an inverse relationship is observed between sheet thickness and springback, where thicker sheets demonstrate lower springback values due to their reduced elastic recovery capacity. For R = 2 mm (a), the highest springback is observed in the t = 1 mm thick sample. In the cases of R = 3 mm and R = 4 mm (b and c), the maximum springback typically occurs in thinner sheets, particularly those with t = 1 or 2 mm. These findings reveal that springback behaviour is highly sensitive to both sheet thickness and punch radii, emphasising the importance of optimising these parameters in precision sheet metal forming processes.

In the present study, the nominal bending angle refers to the target opening angle after unloading. Therefore, smaller bending angles (e.g., 15°) require much deeper punch penetration and generate higher plastic strain, whereas larger angles (e.g., 120°) are achieved with shallower punch displacement and lower plastic deformation. Despite this reduction in plastic strain at larger bending angles, the observed springback increases because the effective bending arm becomes longer and the geometric constraint diminishes, leading to higher residual bending moments during unloading. This geometric effect dominates over the reduction in plastic strain and explains why springback increases with the bending angle without contradicting the mechanics of the V-bending process.

The Finite Element Method is widely used to simulate complex bending processes and gives successful results in predicting deformation behaviour [14]. One of the most important factors affecting the accuracy of this method is the number and type of mesh used in the model. A higher number of mesh elements increases the precision by allowing the geometry to be divided into smaller parts, which improves the level of detail in the analysis. However, finer mesh structures increase the computational time significantly, even when a half-model is used to reduce the processing load (see Section 4, Fig. 7). The comparison between the experimental and FEM results shows strong overall agreement, with a Mean Absolute Error of 0.49° and an RMSE of 0.72°, both calculated directly from the full experimental-FEM dataset evaluated in this study. These low error levels confirm that the numerical model captures springback behaviour with high accuracy across a wide range of bending conditions. Although some local differences appear at both low and high bending angles when small punch radii are used, the FEM predictions remain consistent with the experimental trend. Therefore, selecting the appropriate mesh size and structure is critical for achieving reliable results. These error metrics demonstrate that the FEM model provides reliable and quantitatively validated predictions of springback across the investigated parameter range. This confirms that FEM provides a trustworthy mathematical approach for estimating deformation and springback behaviour in sheet bending processes.

In addition to FEM, artificial neural networks have also been recognised in the literature as effective tools for predicting springback and other bending parameters [19–23, 24, 26–27]. When properly trained, these models can provide fast and accurate predictions, and they are suitable for use in production environments. In the following section, the artificial neural network model developed in this work will be introduced and its performance is compared with the experimental results.

5. ANN prediction model

ANN has become an important tool in solving engineering problems that are difficult to predict in advance, especially springback, thanks to its ability to analyse complex datasets. Estimating intermediate values that cannot be obtained with traditional methods but are of critical importance has become feasible due to the modelling capabilities offered by ANN. In this study, a network architecture consisting of three inputs, two hidden layers with five neurons, and one output layer was used within the Artificial Neural Networks (ANN) framework to estimate springback variations (Fig. 12).

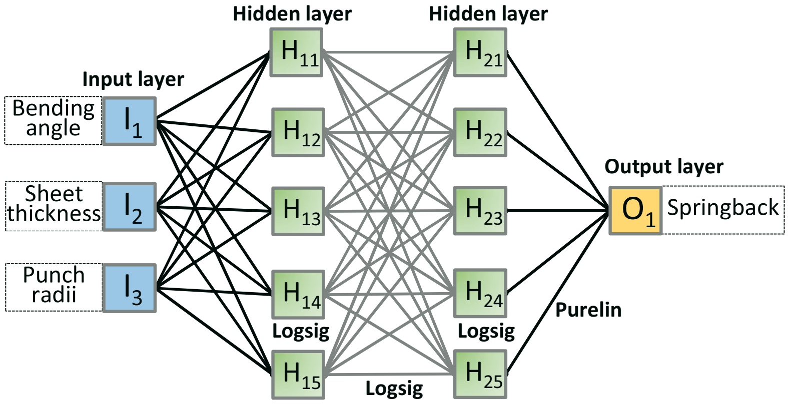

Fig. 12 Artificial Neural Networks (ANN) architecture used in the study

While the logarithmic sigmoid function was applied between the input and hidden layers, the Purelin function was used in the output layer. In the artificial neural network (ANN) model developed here, the logsig activation function was employed to capture nonlinear patterns between the inputs and hidden layers, while the Purelin (linear) function was utilised in the output to produce continuous numerical predictions. The logsig function maps input values into a bounded interval, enabling the network to represent nonlinear dependencies inherent in springback behaviour. It is defined mathematically as:

$$f(x)=\frac{1}{1+e^{-x}}. \tag{2}$$

This function is particularly useful in hidden layers as it introduces nonlinearity, allowing the network to approximate a wide range of nonlinear functions. On the other hand, the Purelin function is a linear activation function defined as:

$$f(x)=x. \tag{3}$$

This is commonly adopted in regression neural networks where a continuous output is required rather than a categorical one. The combined use of nonlinear activation in the hidden layers and a linear function at the output enables the ANN to represent input-springback interactions consistently. During training, the network weights were updated according to the error magnitude so that predicted values gradually converged toward their targets. A total of 106 experimental measurements were used as the dataset. A 70-15-15 split was adopted for training, testing, and validation, respectively, to maximise the number of samples available for weight optimisation while retaining independent subsets for validation and final performance evaluation — a partitioning strategy widely applied in small-to-medium engineering datasets [20, 27]. It should be noted that 106 samples are relatively limited for a three-input ANN spanning four thickness levels, seven bending angles, and three punch radii, which yields 84 unique parameter combinations and an average of only ~1.26 samples per combination. This constraint is reflected in the higher deviations observed at small bending angles, where the elastic-plastic boundary is most sensitive. Expanding the dataset through targeted sampling at underrepresented parameter combinations would substantially improve prediction stability and generalisation. Furthermore, the adoption of k-fold cross-validation in future work would provide a more robust assessment of model generalisation, particularly given the limited dataset size. The comparison of actual and predicted values obtained during training is presented in Fig. 13.

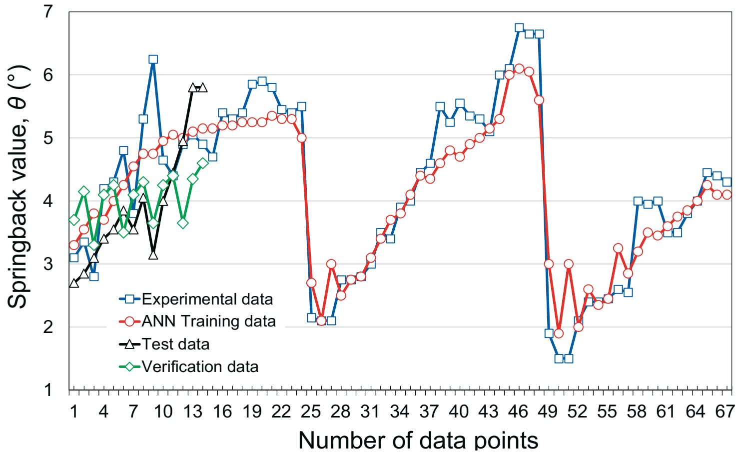

Fig. 13 ANN training validation graph: experimental (○), training (□), test (×), and validation (◇) data

All calculations and the system architecture related to the ANN model were carried out using the artificial neural networks module of MATLAB® software. The correlation coefficients obtained from the training process are presented in Fig. 14. The correlation between the predicted outputs and the target values is indicated by the regression results. In the regression graphs below, the network responses for the training, validation, and test sets can be compared with their corresponding targets. Accordingly, Fig. 14a illustrates the regression analysis of the training data; Fig. 14b shows the regression analysis for the validation set; Fig. 14c displays the regression analysis for the test data; and Fig. 14d provides the overall regression curve for the proposed ANN. The correlation coefficients were calculated as 0.94116 for training, 0.93352 for validation, 0.87525 for testing, and 0.93107 for the entire dataset. Since all correlation values are close to 1, they confirm a strong relationship between the predicted outputs and the actual values. As a result, the artificial neural network model was able to capture the relationship between the input parameters and the output parameter. In this paper, deviation values (%) were determined using the relative error (RE) method [27] to evaluate the ANN performance.

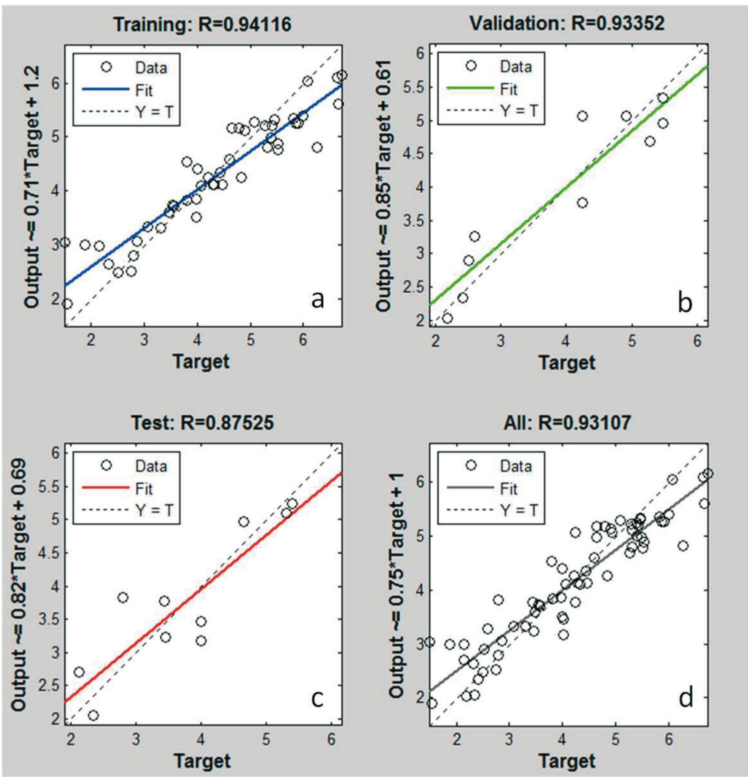

Fig. 14 Correlation coefficients of training series

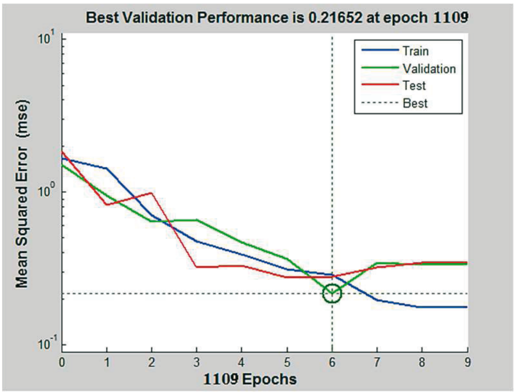

Fig. 15 Mean Square Error (MSE) of the ANN model

During network training, the weights were updated until the error value reached 1.12×10^{-1}. The figure shows the evolution of error performance during the training phase. As seen in Fig. 15, the model converged after six iterations, at which point the error metric reached its optimal value. In comparing the present ANN predictions with previously collected experimental results, very close numerical values were obtained. This indicates that the ANN was able to represent the experimental data with sufficient accuracy. When Fig. 16 is examined, deviations appear at the initial bending angles of 15° and 30° (yet remain within ±15% across all test samples), whereas at 45°, 60°, 90°, and 120°, the ANN results closely match the experimental measurements. Increasing the number of samples is essential for producing more stable and convergent ANN predictions. As reflected in the graph, it can be anticipated that deviation values will approach the horizontal axis and move toward zero as the sample size increases.

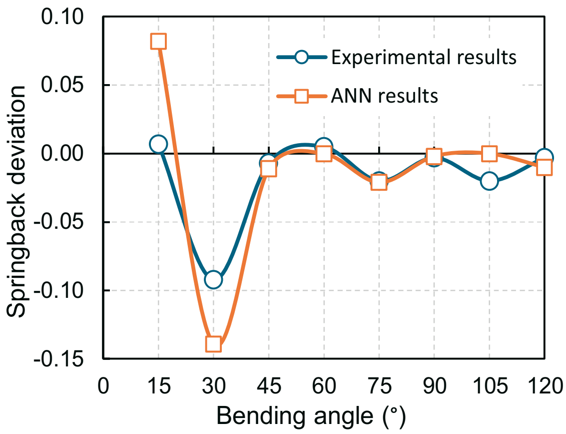

Fig. 16 Comparison of experimental results vs ANN results for t=1@R=1

Figures 17a–17m present the variation in springback as a function of bending angle for different combinations of sheet thickness (t = 1–4 mm) and punch radius (R = 1–8 mm). Each subfigure provides a comparative view of the experimental measurements together with the predictions obtained from the FEM and ANN models. Across all conditions, a consistent trend is observed in which springback increases as the bending angle becomes larger. This behaviour agrees with established expectations, since higher bending angles are generally associated with greater elastic recovery resulting from accumulated strain within the material.

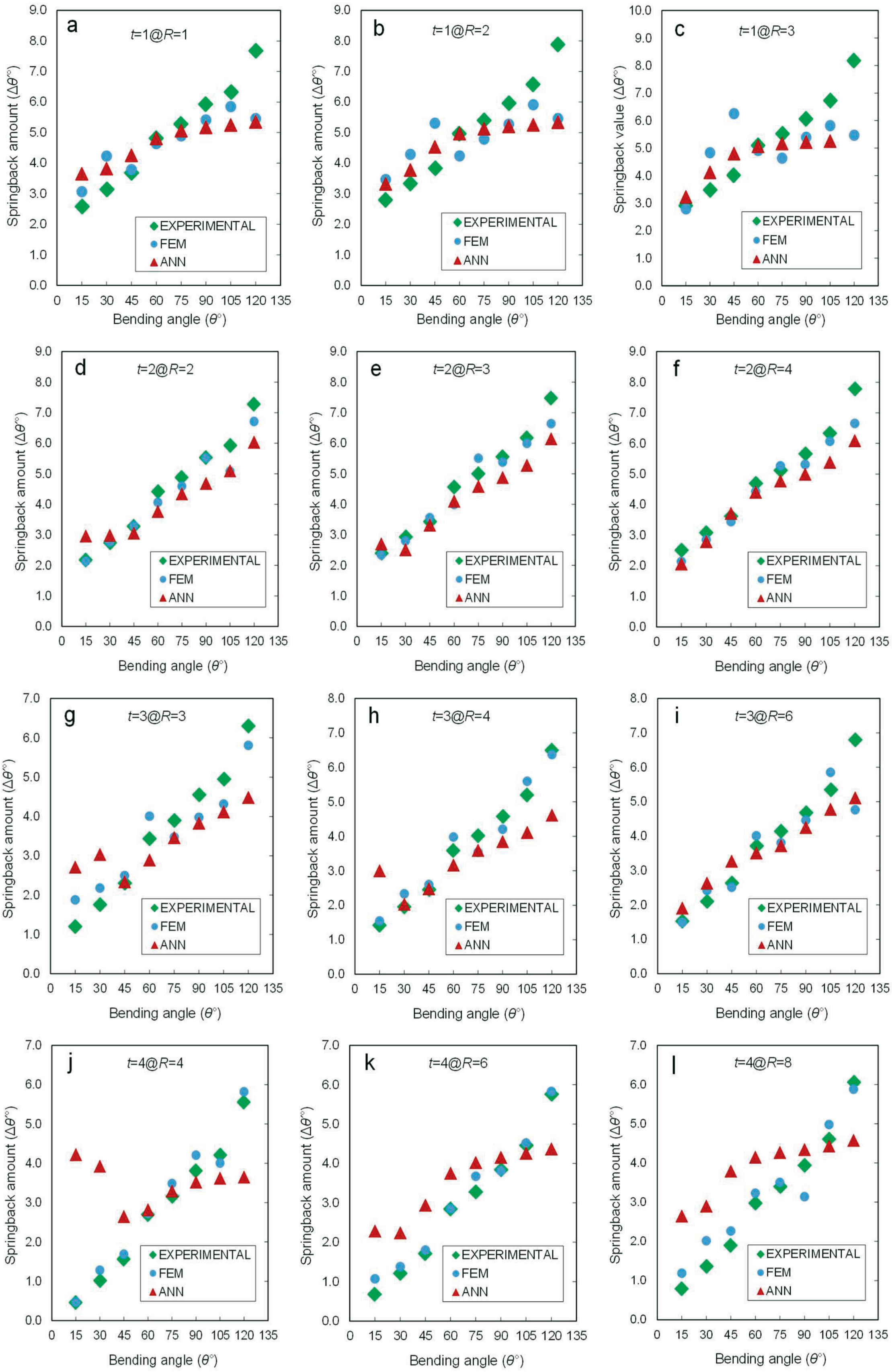

Fig. 17 Experimental, FEM, and ANN comparisons for t = 1–4 mm sheets under three bending radii

For thinner sheets (e.g., t = 1 mm; Fig. 17a–17c), FEM tends to slightly overestimate springback at higher bending angles, whereas ANN predictions often remain closer to the experimental data. As sheet thickness increases (t = 2–4 mm), the ANN model generally continues to reflect the experimental trend, although noticeable deviations appear when larger punch radii are considered (Fig. 17j–17l). These differences may arise from nonlinear deformation behaviour or complex strain distributions that are more difficult to capture accurately using data-driven methods alone. The ANN model produces relatively smooth prediction curves and demonstrates good generalisation capability across the full bending range. Nevertheless, small underestimations can be observed at lower angles in specific cases (e.g., Fig. 17g and 17h), which could be reduced by expanding the training dataset with additional localised measurements.

FEM results show good consistency with experiments at intermediate angles but may diverge under more extreme bending conditions. Overall, the ANN and FEM approaches complement one another and, when combined with experimental observations, they provide a balanced and effective framework for estimating springback in sheet metal forming applications.

6. Hybrid GA-ANN model for optimised springback prediction

Artificial Neural Networks have become an effective tool for modelling complex physical behaviour, particularly springback in sheet metal forming. However, classical ANN models trained with backpropagation may converge to local minima because of random weight initialisation, which weakens generalisation on unseen data. To overcome this limitation, a Genetic Algorithm (GA) was integrated into the ANN framework, creating a hybrid GA-ANN model.

Genetic Algorithms are evolutionary optimisation techniques capable of locating global optima in multidimensional nonlinear search spaces. In this study, GA was used to optimise the ANN weight and bias parameters rather than relying solely on gradient-based learning. By exploring the solution space broadly, GA determined more suitable initial conditions for ANN training and contributed to reducing the Mean Squared Error (MSE). Each individual in the GA population represented a complete weight-bias vector, and the MSE from ANN predictions served as the fitness function. The population evolved through crossover, mutation, and selection operations, with parameters (population size, mutation rate, number of generations) determined experimentally to achieve stable convergence.

In this hybrid framework, GA does not analyse the dataset directly. Instead, it functions as an evolutionary optimiser that determines the initial weight and bias configuration of the ANN. The GA hyperparameters (population = 50, mutation rate = 0.05, crossover rate = 0.8, generations = 100) were selected through preliminary sensitivity trials as the combination yielding stable MSE convergence at acceptable computational cost, consistent with comparable GA-ANN studies [27, 32]. A mutation rate of 0.05 was used to preserve diversity in the population, while a crossover rate of 0.8 facilitated an effective recombination of candidate solutions. Tournament selection was adopted as the selection strategy due to its stable convergence behaviour. The optimisation was carried out for 100 generations, after which no further reduction in MSE was observed. The optimal individual obtained at the end of this evolutionary process was then used to initialise the ANN weights and biases, enhancing network stability and improving prediction accuracy.

The Hybrid Genetic Algorithm-Artificial Neural Network (GA-ANN) model therefore combines the global search capability of GA with the nonlinear learning capacity of ANN. The ANN architecture used in this study is a feedforward network consisting of three input parameters (x_1, x_2, x_3), two hidden layers, and a single output neuron. The general mathematical representation of the model is given as follows [28]:

$$\hat{y} = f_{\text{output}}\left(\sum_{j=1}^{n_h} w_j^{(2)} \cdot f_{\text{hidden}}\left(\sum_{i=1}^{n_{in}} w_{ji}^{(1)} \cdot x_i + b_j^{(1)}\right) + b^{(2)}\right), \tag{4}$$

where x_i denotes the input parameters (sheet thickness, bending angle, and punch radius), $\omega_{ij}^{(1)}$ and $b_j^{(1)}$ are the weights and biases of the hidden layers, $\omega_j^{(2)}$ and $b^{(2)}$ are the weights and biases of the output layer, f_{hidden} and f_{output} refer to the log-sigmoid and linear (Purelin) activation functions, respectively, and $\hat{y}$ is the predicted springback amount.

$$MSE = \frac{1}{n}\sum_{i=1}^{n}(y_i - \hat{y}_i)^2 \tag{5}$$

The GA optimisation process aims to determine the optimal weights and bias values that minimise the Mean Squared Error (MSE), as defined by the above equation (5) [30]. Each GA individual (chromosome) represents a candidate weight-bias vector [30]:

$$K = \left[w^{(1)}, b^{(1)}, w^{(2)}, b^{(1)} \right]. \tag{6}$$

The fitness of each individual is evaluated based on the defined error function. The genetic algorithm (GA) proceeds through several evolutionary steps, including selection, where the most suitable individuals are chosen for the next generation, using methods such as roulette wheel or tournament selection; crossover, in which new individuals are produced by combining genetic information from selected pairs; and mutation, where small random alterations are introduced to maintain diversity within the population. The optimal individual K^*, identified at the end of this evolutionary process, is assigned as the initial configuration for the ANN model. The prediction phase is then performed using these optimised parameters, resulting in more accurate and reliable estimations with reduced error.

The model performance was evaluated in comparison with the conventional ANN approach, and it was observed that the GA-ANN model outperformed the standard ANN in both training and test datasets by achieving higher correlation coefficients (R^2) and lower MSE values. These findings indicate that GA-based optimisation not only enhances the predictive accuracy but also improves the structural stability of the ANN model. The results obtained (Table 3) demonstrate that the proposed hybrid model provides a reliable and optimised approach, achieving an MAE of 0.075° and MSE of 0.011 compared to 0.195° and 0.059 for the conventional ANN, representing a 61.5% reduction in MAE and a five-fold improvement in MSE. The corresponding comparative performance metrics are detailed in Table 4, while the prediction accuracy is illustrated graphically in Fig. 18. These metrics were calculated based on the full test set of 14 samples (~15% of 106 total measurements). Table 3 presents 14 representative samples selected to illustrate the range of prediction accuracy; the complete test set results are consistent with the reported aggregate metrics.

Table 3 GA-ANN estimation results

No	Train-target	Train-predicted	Test-target	Test-predicted	Relative Error (%)
1	3.071	3.321	3.121	3.300	5.73
2	3.464	3.228	3.413	3.352	1.78
3	2.796	3.822	2.752	2.895	5.19
4	4.236	3.772	4.154	4.496	8.23
5	4.286	4.120	4.253	4.104	3.50
6	4.838	4.257	4.920	4.488	8.78
7	3.792	4.529	3.788	3.593	5.15
8	5.310	4.797	5.086	4.414	13.21
9	6.256	4.812	6.279	6.650	5.90
10	4.646	4.966	4.605	4.953	7.55
11	4.236	5.067	4.211	3.789	10.02
12	4.918	5.062	5.011	5.114	2.05
13	4.898	5.125	4.952	4.942	0.20
14	4.784	5.166	4.798	4.552	5.12

Table 4 Comparative performance results of ANN and GA-ANN models

Model Type	R^2 (Training)	R^2 (Test)	Mean Squared Error (MSE)	Mean Absolute Error (MAE)
ANN	0.931	0.833	0.059	0.195
GA-ANN	0.965	0.875	0.011	0.075

Figure 18 illustrates the comparative performance of the Genetic Algorithm-optimised Artificial Neural Network (GA-ANN) model against the actual experimental springback values obtained from the test data. The plot reveals that the GA-ANN model successfully captures the general trend and non-linear behaviour of springback across various test samples. Particularly between samples 1 and 8, the predicted values closely follow the actual measurements with minimal deviation, demonstrating the model's ability to approximate the springback phenomenon accurately under different bending conditions. In the latter part of the data series (samples 9–14), some fluctuations between the predicted and actual values are observed.

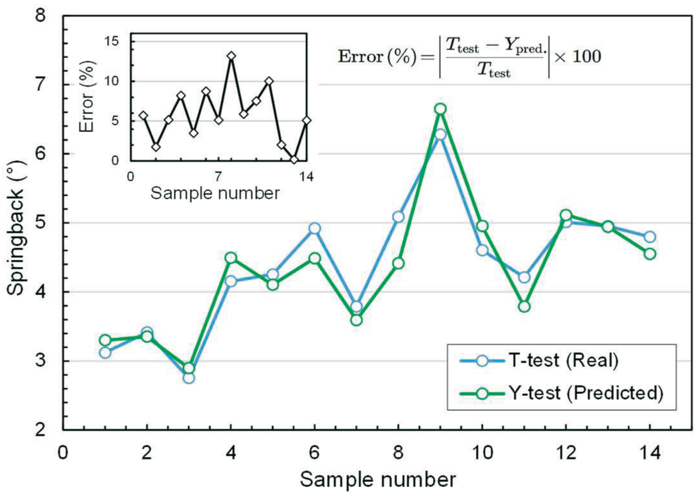

Fig. 18 Actual and predicted springback values for the GA-ANN model with inset showing relative error (%) per test sample

These discrepancies may be attributed to localised effects such as strain hardening, material anisotropy, or minor misalignments during the physical bending process, which are not fully accounted for in the model's training data. Despite these slight deviations, the GA-ANN predictions remain within a reasonable margin of error, indicating that the model does not suffer from overfitting and retains strong generalisation capabilities.

Future work may extend the proposed framework by incorporating physics-informed neural networks [35] and real-time closed-loop springback compensation strategies [36]. Applying deep learning architectures to larger FEM-generated datasets [37] and exploring springback prediction across diverse automotive-grade materials [38] would further improve generalisation. Additionally, integrating advanced optimisation algorithms beyond GA may enhance both convergence speed and prediction robustness across wider forming condition ranges.

7. Conclusions

This study establishes an integrated framework combining experimental measurements, finite element simulations, and a GA-optimised ANN for accurate springback prediction in air V-bending of mild steel sheets. The experimental results confirmed that springback increases systematically with the bending angle and punch radius, while it decreases with sheet thickness across all investigated parameter combinations. The FEM model showed strong quantitative agreement with the experiments, achieving an MAE of 0.49° and an RMSE of 0.72°, thereby validating its reliability as a physics-based reference model.

A feedforward ANN trained on 106 experimental samples achieved a correlation coefficient of 0.93, demonstrating that data-driven modelling can successfully capture nonlinear parameter interactions without repeated numerical simulations. The integration of a Genetic Algorithm for ANN weight initialisation further enhanced predictive performance, increasing test R^2 from 0.833 to 0.875, reducing MAE from 0.195° to 0.075° (61.5% improvement), and MSE five-fold from 0.059 to 0.011. These results confirm that GA-enhanced initialisation substantially improves both prediction accuracy and convergence stability.

Overall, the proposed hybrid framework provides a computationally efficient and industrially applicable alternative to iterative FEM-based springback compensation, supporting tool design and process optimisation in sheet metal forming. Future research may expand the dataset, incorporate anisotropic hardening models, and explore advanced evolutionary strategies to further strengthen generalisation capability.

Data Availability Statement

The data generated and analysed during this study are available from the corresponding author upon reasonable request and subject to institutional regulations.

REFERENCES

[1] Tongxi Y., Zhang L. Plastic bending: Theory and Applications, **1996**, Vol. 2. World Scientific.

[2] Civelek F., Özdemir A. Evaluation of formability criteria for sheet metal materials, J. Polytech. **2024** 27(4):1617-1631. https://doi.org/10.2339/politeknik.1392287

[3] Inamdar M.V., Date P.P., Sabnis S.V. On the effects of geometric parameters on springback in sheets of five materials subjected to air vee bending, J. Mater. Process. Technol. **2002**, 123:459-463. https://doi.org/10.1016/S0924-0136(02)00136-X

[4] Yaman K., Özcan M., Tekiner Z. Determination of the spinning parameters of AISI 304L stainless steel by using Finite Element Method, J. Fac. Eng. Archit. Gazi Univ. **2018**, 33(1):299-311. doi.org/10.17341/gazimmfd.406802

[5] Leu D.K., Zhuang Z.W. Springback prediction of the vee bending process for high-strength steel sheets, J. Mechanical Eng. Sci. Technol. **2016**, 30(3):1077-1084. https://doi.org/10.1007/s12206-016-0212-8

[6] Hai V.G., Minh N.T.H., Nguyen D.T. A study on experiment and simulation to predict the springback of SS400 steel sheet in large radius V-bending process, Mater. Res. Express. **2020**, 7:016562. https://doi.org/10.1088/2053-1591/ab67f5

[7] Asnafi N. Springback and fracture in V-die air bending of thick stainless steel sheets, Mater. Des. **2000**, 21:217-236. https://doi.org/10.1016/S0261-3069(99)00051-5

[8] Streppel A.H., De Vin L.J., Brinkman J., Kals H.J.J. Suitability of sheet bending modelling techniques in CAPP applications, J. Mater. Process. Technol. **1993**, 36:339-356. https://doi.org/10.1016/0924-0136(93)90038-8

[9] Zhang C., Lou Y. Influences of the evolving plastic behavior of sheet metal on V-bending and springback analysis considering different stress states, Int. J. Plast. **2024**, 173:103889. https://doi.org/10.1016/j.ijplas.2024.103889

[10] Tekiner Z. An experimental study on the examination of springback of sheet metals with several thicknesses and properties in bending dies, J. Mater. Process. Technol. **2004**, 145:109-117. https://doi.org/10.1016/j.jmatprotec.2003.07.005

[11] Gattmah J., Ozturk F., Orhan S. Numerical simulation of bending process for steel plate using finite element analysis, Arab. J. Sci. Eng. **2019**, 44:10285-10292. https://doi.org/10.1007/s13369-019-04119-8

[12] Fei D., Hodgson P. Experimental and numerical studies of springback in air V-bending process for cold rolled TRIP steels, Nucl. Eng. Des. **2006**, 236:1847-1851. https://doi.org/10.1016/j.nucengdes.2006.01.016

[13] Ling Y.E., Lee H.P., Cheok B.T. Finite element analysis of springback in L-bending of sheet metal, J. Mater. Process. Technol. **2005**, 168(2):296-302. https://doi.org/10.1016/j.jmatprotec.2005.02.236

[14] Badr O.M., Rolfe B., Zhang P., Weiss M. Applying a new constitutive model to analyse the springback behaviour of titanium in bending and roll forming, Int. J. Mech. Sci. **2017**, 128-129:389-400. https://doi.org/10.1016/j.ijmecsci.2017.05.025

[15] Karabulut S., Esen İ., Şahin E. Springback prediction performance and experimental analysis in the V-bending process of SCGADUB1180 advanced high-strength steel, Jordan J. Mech. Ind. Eng. **2024**, 18(2):441-453. https://doi.org/10.59038/jjmie/180216

[16] Chen P., Lu S. Springback characteristics and influencing laws of four-axis flexible roll bending forming for aluminum alloy, PLoS One. **2024**, 19(8):0-17. https://doi.org/10.1371/journal.pone.0306604

[17] Hayrat K., Kosa E., Durmuşoğlu Ş. An experimental investigation of formability of Inconel sheet plate for different die angles and rolling directions in press brake bending, Eur. Mech. Sci. **2023**, 7(1):29-34. https://doi.org/10.26701/ems.1132428

[18] Trieu Q.H., Vuong G.H., Nguyen D.T. Predictive modeling of springback behavior in V-bending of SS400 steel sheets under elevated temperatures using combined hardening laws, Appl. Sci. **2023**, 13:10347. https://doi.org/10.3390/app131810347

[19] Inamdar M.V., Date P.P., Desai U.B. Studies on the prediction of springback in air vee bending of metallic sheets using an artificial neural network, J. Mater. Process. Technol. **2000**, 108(1):45-54. https://doi.org/10.1016/S0924-0136(00)00588-4

[20] Forcellese A., Gabrielli F., Ruffini R. Effect of the training set size on springback control by neural network in an air bending process, J. Mater. Process. Technol. **1998**, 80-81:493-500. https://doi.org/10.1016/S0924-0136(98)00122-8

[21] Asmael M., Fubara O.T., Nasir T. Prediction of springback behavior of vee bending process of AA5052 aluminum alloy sheets using machine learning, Jordan J. Mech. Ind. Eng. **2023**, 17(1):1-14. https://doi.org/10.59038/jjmie/170101

[22] Bozdemir M., Gölcü M. Artificial neural network analysis of springback in V-bending, J. Appl. Sci. **2008**, 8(17):3038-3043. https://doi.org/10.3923/jas.2008.3038.3043

[23] Özdemir M. Optimization of springback in air V-bending processing using Taguchi and RSM method, Mechanika. **2020**, 26(1):73-81. https://doi.org/10.5755/j01.mech.26.1.22831

[24] Yang Y., Chalal H., Baudouin C., Vincze G., Balan T. Prediction of springback after bending under tension, Int. J. Mater. Form. **2022**, 15:34. https://doi.org/10.1007/s12289-022-01689-1

[25] Miranda S.S., Barbosa M.R., Santos A.D., Pacheco J.B., Amaral R.L. Forming and springback prediction in press brake air bending combining finite element analysis and neural networks, J. Strain Anal. Eng. Des. **2018**, 53:584-601. https://doi.org/10.1177/0309324718798222

[26] Serban F.M., Grozav S., Ceclan V., Turcu A. Artificial neural networks model for springback prediction in bending operations, Teh. Vjesn. **2020**, 27(3):868-873. https://doi.org/10.17559/TV-20141209182117

[27] Trzepieciński T., Lemu H.G. Improving prediction of springback in sheet metal forming using multilayer perceptron-based genetic algorithm, Materials. **2020**, 13(14):3129. https://doi.org/10.3390/ma13143129

[28] Xu B., Li L., Wang Z., Zhou H., Liu D. Prediction of springback in local bending of hull plates using an optimized backpropagation neural network, Mech. Sci. **2021**, 12:777-789. https://doi.org/10.5194/ms-12-777-2021

[29] Xu Z., Qiu D., Shahzamanian M.M., Zhou Z., Mei D., Peng L. An improved springback model considering the transverse stress in microforming, Int. J. Mech. Sci. **2023**, 241:107947. https://doi.org/10.1016/j.ijmecsci.2022.107947

[30] Bingqian Y., Zeng Y., Yang H., Oscoz M.P., Ortiz M., Coenen F., Nguyen A. Springback prediction using point series and deep learning, Int. J. Adv. Manuf. Technol. **2024**, 132:4723-4735. https://doi.org/10.1007/s00170-024-13632-6

[31] Wasif M., Rababah M., Fatima A., Baig S.U.R. Prediction of springback using machine learning techniques in high-tensile-strength sheet metal during the V-bending process, Jordan J. Mech. Ind. Eng. **2023**, 17(4):481-488. https://doi.org/10.59038/jjmie/170403

[32] Duan Y., Tian L., Zhang F., Liu Y., Qiao H., Yang L., Guan Y. Precision and flexible bending control strategy based on analytical and data-driven models, Chin. J. Mech. Eng. **2022**, 35:107. https://doi.org/10.1186/s10033-022-00772-7

[33] Karalar M., Bayramoğlu M. Simultaneous effects of temperature, holding time and thickness on bending springback of DP1000 steel: experiments and statistical analysis, Sci. Rep. **2025**, 15:37192. https://doi.org/10.1038/s41598-025-18308-z

[34] Karakaya Ç., Ekşi S. Springback behavior of AA7075-T6 alloy in V-shaped bending, Appl. Sci. **2025**, 15:5509. https://doi.org/10.3390/app15105509

[35] Xu J., Yan J., Huang Y., Ding D. Simulation and prediction of springback in sheet metal bending process based on embedded control system, *Sensors*. **2024**, 24:7863. https://doi.org/10.3390/s24237863

[36] Molitor D.A., Arne V., Kubik C., Neomark G., Groche P. Inline closed-loop control of bending angles with machine learning supported springback compensation, Int. J. Mater. Form. **2024**, 17:8. https://doi.org/10.1007/s12289-023-01802-y

[37] Cu S., Sun Y., Wu K. Machine learning methods for springback control in roll forming, Int. J. Mater. Form. **2025**, 18:7. https://doi.org/10.1007/s12289-024-01872-6

[38] Spišák E., Majerníková J., Mulidrán P. Hajduk J., Ruda F. Springback analysis and prediction of automotive steel sheets used in compression bending, Materials. **2025**, 18:774. https://doi.org/10.3390/ma18040774

Submitted: 18.12.2025

Accepted: 16.3.2026

Kemal Yaman*
OSTİM Technical University, Industrial Design Department, 06374, Ankara, Turkey

Zafer Tekiner
Gazi University, Technology Faculty, Department of Manufacturing Engineering, Ankara, Turkey

*Corresponding author:
kemal.yaman@ostimteknik.edu.tr